LANGMUIR Article
Cite This: Langmuir 2018, 34, 4427−4436
pubs.acs.org/Langmuir

Individually Dispersed Gold Nanoshell-Bearing Cellulose Nanocrystals with Tailorable Plasmon Resonance

Nikolay S. Semenikhin,[†,§] Naveen Reddy Kadasala,[⊥] Robert J. Moon,[†,‡,§] Joseph W. Perry,[∥] and Kenneth H. Sandhage*[,⊥]

[†]School of Materials Science and Engineering, [§]Renewable Bioproducts Institute, and [∥]School of Chemistry and Biochemistry, Georgia Institute of Technology, Atlanta 30332, Georgia, United States

[‡]The Forest Product Laboratory, US Forest Service, Madison 53726, Wisconsin, United States

[⊥]School of Materials Engineering, Purdue University, 701 West Stadium Avenue, West Lafayette 47907, Indiana, United States

ABSTRACT: Cellulose nanocrystals (CNCs) can be attractive templates for the generation of functional inorganic/organic nanoparticles, given their fine sizes, aspect ratios, and sustainable worldwide availability in abundant quantities. Here, we present for the first time a scalable, surfactant-free, tailorable wet chemical process for converting commercially available CNCs into individual aspected gold nanoshell-bearing particles with tunable surface plasmon resonance bands. Using a rational cellulose functionalization approach, stable suspensions of positively charged CNCs have been generated. Continuous, conductive, nanocrystalline gold coatings were then applied to the individual, electrostatically stabilized CNCs via decoration with 1−3 nm diameter gold particles followed by electroless gold deposition. Optical analyses indicated that these core−shell nanoparticles exhibited two surface plasmon absorbance bands, with one located in the visible range (near 550 nm) and the other at near infrared (NIR) wavelengths. The NIR band possessed a peak maximum wavelength that could be tuned over a wide range (1000−1300 nm) by adjusting the gold coating thickness. The bandwidth and wavelength of the peak maximum of the NIR band were also sensitive to the particle size distribution and could be further refined by fractionation using viscosity gradient centrifugation.

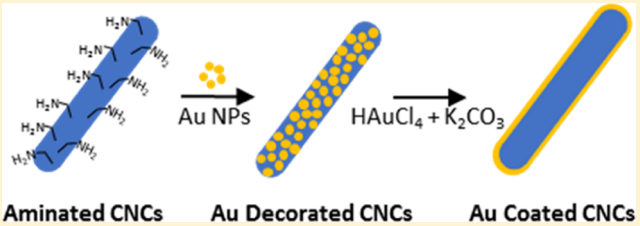

INTRODUCTION

As the uses of nanoparticles and nanoparticle-bearing assemblies continue to expand in an increasing variety of applications,[1−4] the development of sustainable, scalable, and cost-effective fabrication techniques that allow for tailorable particle chemistries, structures, and properties is becoming increasingly more important. A common approach among the synthesis strategies examined to date has been to chemically tailor a template possessing a desired morphology that can be generated in large quantities.[5] Certain nanoscale or nanostructured biogenic particles are formed in a massively parallel and sustainable manner, which makes such particles particularly attractive for use as templates. For example, diatom frustules,[6−12] bacteria,[13] DNA,[14] virus particles,[15,16] and cellulose nanocrystal (CNC) assemblies[17−19] have been chemically altered via conformal coating and/or reactive transformation methods to endow such structures with new properties.

The syntheses of functional metallic/organic nanostructures via metal deposition onto sustainable bio-organic templates (e.g., bacteria, virus particles, and CNC assemblies) have been examined by a number of authors.[13−21] Gold nanoparticle-bearing structures have been of particular interest for use in a variety of fields (e.g., optoelectronics,[22,23] nanomedicine,[24] chemical sensing,[25] and catalysis[26]) owing to their shape- and size-dependent optical properties, biocompatibility, catalytic activity, and chemical inertness. Aspected gold nanostructures (nanorods, nanotubes) offer the potential for tailorable optical behavior, such as tunable surface plasmon resonance and scattering, via adjustment of the particle length and diameter/wall thickness to affect several surface plasmon resonance modes. Indeed, aspected gold-bearing nanostructures may be synthesized with optical extinction bands at near infrared (NIR) wavelengths, which encompasses biological windows of optical transparency (650−900 and 1000−1350 nm), for use as probes for in vitro and in vivo imaging (e.g., via photoacoustic, two-photon luminescence, and darkfield modalities).[27,28] The absorption of NIR light by localized gold nanoparticles and conversion into heat can also be an effective means of killing cancerous cells without damaging the surrounding tissue (photothermal cancer therapy).[29−32] The high density of gold has also enabled gold nanoparticles to be effective contrast agents in X-ray tomography for tracking the cell movement, fluid flow, and tumor growth in live specimens.[33−35]

In this paper, we demonstrate for the first time the use of commercially available CNCs as sustainable biotemplates for the syntheses of singly dispersed, aspected gold nanoshell-bearing particles with tunable optical properties using a

Received: November 9, 2017
Revised: January 30, 2018
Published: March 26, 2018

DOI: 10.1021/acs.langmuir.7b03868
Langmuir 2018, 34, 4427−4436

scalable, aqueous, surfactant-free, wet chemical process. CNCs can be isolated from cellulose (earth's most abundant biopolymer) generated by plants, animals (e.g., tunicates), and bacteria.[36,37] Such biogenic CNCs have a high aspect ratio and rod-like morphology (5−20 nm diameter, 25−3000 nm length) and possess a surface amenable for chemical modification.[37,38] In the present work, a rational CNC surface functionalization approach has been used to create stable CNC suspensions having a high affinity for gold nanoparticles which, upon binding, serve as heterogeneous nucleation sites for subsequent electroless deposition of additional gold to yield continuous nanocrystalline gold coatings on individual CNC particles. Previous attempts to create dense, continuous, and conformal gold coatings on CNCs have yielded materials exhibiting broad optical extinction that is characteristic of plasmonic nanoparticle aggregates.[39,40] Indeed, the tendency of CNCs to form hydrogen-bonded networks is well documented and has been exploited to generate high surface area aero/hydrogel templates for the deposition of randomly dispersed gold nanoparticles for catalysis and chemical sensing applications.[17,18] The present work instead provides a readily scalable means of synthesizing individual aspected gold nanoshell-bearing CNC particles with tailorable optical extinction at NIR wavelengths. This CNC functionalization and templating process avoids the appreciable retention of cytotoxic surfactants (such as cetyltrimethylammonium bromide) commonly used in the syntheses of gold nanorods, which is a distinct advantage for biological/biomedical applications because additional ligand exchange is not required.[41]

EXPERIMENTAL SECTION

Removal of Sulfate Esters. An aqueous CNC slurry (11.8 wt % CNCs, lot#: 2014-FPL-CNC-064, produced at USDA Forest Products Laboratory, Madison, WI) was obtained from the Process Development Center at the University of Maine (Orono, ME). Sulfate ester groups present on the as-received CNCs were removed by acid hydrolysis. A 1.0 wt % stock CNC suspension was prepared by diluting the 11.8 wt % aqueous commercial CNC slurry with deionized (DI) water (NANOpure, Barnstead International, Dubuque, IA). Hydrochloric acid (37 wt %) was added to 300 mL of the 1.0 wt % suspension to achieve a molarity of 0.25 M. The acidic suspension was then heated under reflux at 100 °C under magnetic stirring (250 rpm, magnetic stirring hot plate, Cimarec, Barnstead International, Dubuque, IA) for 24 h in a 500 mL round-bottom flask. After cooling, the CNCs were washed by repeated centrifugation [relative centrifugal force (RCF), of 8000, 5 min] and redispersion in DI water using a vortexer (Vortex-Genie 2T, Bohemia, NY) until the pH of the supernatant reached a value of 6. The CNCs were then dispersed in 200 mL of DI water using the vortexer. The suspension was probe sonicated (Misonix 3000, Misonix Inc., Farmingdale, NY) at 30% of the peak amplitude for 5 min to break up agglomerates. The suspension was then transferred to dialysis bags (14 000 MWCO, Ward's Science, Rochester, NY) and dialyzed against DI water to a neutral pH. The resulting opaque, milky suspension of desulfonated CNCs was diluted with the addition of DI water to a CNC content of 0.25 wt % and stored at 4 °C.

Periodate Oxidation. Dialdehyde groups were generated on CNC surfaces by sodium periodate oxidation. Sodium (meta)periodate ($NaIO_4$, 4.0 g, 99% purity, Sigma-Aldrich, St. Louis, MO) was added to a suspension of desulfonated CNCs (200 mL, 0.25 wt % CNC loading). After adjusting the pH of the suspension to 3.5 using glacial acetic acid (99.9% purity, Fisher Scientific, Hampton, NH), the suspension was transferred to a jacketed beaker heated to 45 °C. The beaker was covered with aluminum foil (to avoid exposure to light), and the suspension was magnetically stirred (350 rpm) for 2.5 h in a darkened fume hood. Ethylene glycol (10 mL, 99% purity, BDH VWR Analytical, Radnor, PA) was then added to decompose any remaining periodate to iodate, and after 5 min, the suspension was cooled to room temperature. The suspension was exposed to five cycles of centrifugation (8000 RCF, 5 min) and redispersion in DI water (using a vortexer) to remove excess reagents. After dialysis against DI water (as described above) for 3 days, the resulting dialdehyde-bearing CNC suspension (0.187 wt % CNCs) was stored in a refrigerator at 4 °C.

Reductive Amination. An 80.2 mL suspension of dialdehyde-bearing CNCs (0.187 wt %) was diluted with 80 mL of phosphate buffer (0.2 M, pH 6.0) in a 250 mL round-bottom flask. *N*-Boc-ethylenediamine (1.0 g, 98% purity, Alfa Aesar, Haverhill, MA) and $NaBH_3CN$ (0.4 g, 95% purity, Alfa Aesar, Haverhill, MA) were added to the suspension, which was then magnetically stirred (350 rpm) for 5 days at room temperature. The suspension was exposed to five cycles of centrifugation (8000 RCF, 5 min) and redispersion in DI water (using a vortexer) to remove excess reagents. After the final centrifugation step, the CNCs were suspended in a 4 M HCl solution and magnetically stirred (350 rpm) for 24 h at room temperature to cleave off the Boc protecting group. The CNCs were then washed again by repeated centrifugation and dispersion in DI water (five or more washing cycles) until the supernatant remained turbid from suspended CNCs. After dialysis against DI water to achieve a neutral pH, the amine-bearing CNC (a-CNC) suspension (0.60 wt % a-CNCs) was stored at 4 °C.

Dispersal of a-CNCs. The a-CNC suspension was diluted (from 0.60 to 0.11 wt % a-CNCs) with DI water, and then placed in an ice/water bath for sonication. The a-CNC suspension was sonicated using a 5 mm probe (Misonix 3000, Misonix Inc., Farmingdale, NY) operating in pulse mode (on/off times of 10 s/5 s) at an amplitude of ≈90 μm (power setting of 3) for 2 h [note: further sonication beyond 2 h did not result in a change in the hydrodynamic radius of the a-CNCs, as determined by dynamic light scattering (DLS)].

Preparation of Chloroauric Acid Solution. A stock solution of chloroauric acid ($HAuCl_4$, 99.99% trace metals, Sigma-Aldrich, St. Louis, MO) was prepared at a concentration of 25 mM in DI water. The solution was aged in a dark cabinet for a minimum of 3 days before use.

Preparation of Electroless Au Plating Solution. A chloroauric acid-based electroless gold plating solution was prepared as per the method of Brinson et al.[42] Briefly, the $HAuCl_4$ stock solution (3.0 mL) was mixed with an aqueous solution (200 mL, 1.8 mM) of K_2CO_3 (99% purity, Sigma-Aldrich, St. Louis, MO). The solution was magnetically stirred (350 rpm) for 30 min in a container that was covered with aluminum foil (to avoid exposure to light). The covered solution was then aged in a dark cabinet for a minimum of 24 h before use.

Synthesis of 1−3 nm Diameter Gold Particles. A suspension of 1−3 nm diameter gold particles was prepared as per the method of Duff et al.[43] An aqueous solution of NaOH (0.3 mL, 1 M, ACS Grade, Sigma-Aldrich, St. Louis, MO) was diluted with DI water (47 mL) in a 200 mL beaker. An aqueous solution of tetrakis(hydroxymethyl)-phosphonium chloride (12 μL, 80% THPC, Sigma-Aldrich, St. Louis, MO) was diluted with DI water (1 mL) and then added to the NaOH solution under magnetic stirring (350 rpm). After 5 min, the stirring speed was increased to 1200 rpm, and an aged $HAuCl_4$ solution (1.9 mL, 25 mM) was quickly injected into the THPC−NaOH solution from a pipet (with the aid of a full pipet bulb). The solution quickly turned dark brown in color. After stirring at 1200 rpm for an additional 5 min, the suspension of gold nanoparticles was passed through a 0.1 μm syringe filter into a clean glass bottle (cleaned with aqua regia and thoroughly rinsed with DI water). The gold nanoparticle suspension was stored at 4 °C for a minimum of two weeks before use.

Preparation of Gold Nanoparticle-Decorated a-CNCs. The a-CNC suspension (0.11 wt % a-CNCs) was diluted by adding DI water to increase the suspension volume from 15 μL to 1 mL. The diluted a-CNCs suspension was sonicated for 5 min (Branson 2510 ultrasonic bath, Branson Ultrasonic Corp., St. Louis, MO). The gold nanoparticle suspension (4 mL) was added to a scintillation vial (20 mL, cat no. 66022-065, VWR Analytical, Radnor, PA) that was placed into the

DOI: 10.1021/acs.langmuir.7b03868
Langmuir 2018, 34, 4427−4436

ultrasonic bath. A pipet was used to gradually add the diluted a-CNC suspension (1 mL), at a rate of 0.1 mL per min, to the gold nanoparticle suspension (4 mL). The vial was capped and stored in the dark for 14 h. The gold-decorated a-CNCs were then separated from loose gold nanoparticles by centrifugation. The contents of the scintillation vial were placed into several 2 mL centrifuge vials, and centrifugation was conducted (20 000 RCF) for 30 min. After careful removal of the supernatant, the resulting film of gold-decorated a-CNCs was dispersed in DI water for further centrifugation (15 000 RCF) for 30 min. The DI water dispersal and centrifugation (15 000 RCF) treatment was repeated three more times. The gold-decorated a-CNCs were then placed in 3 mL of DI water and dispersed via exposure to the ultrasonic bath for 1 h. The suspension of gold nanoparticle-decorated a-CNCs (≈0.006 wt % a-CNC loading) was stored at 4 °C.

Carbon Monoxide Generation. Carbon monoxide was generated and used as a reducing agent during electroless gold deposition. Given the odorless, colorless, and toxic nature of carbon monoxide, such carbon monoxide generation and use were conducted entirely within a fume hood. Carbon monoxide was generated in small quantities (500 mL) via the dehydration of 5 mL of formic acid (97% purity, Alfa Aesar, Haverhill, MA) by reaction with 10 mL of sulfuric acid (ACS grade 95−98% purity, BDH VWR Analytical, Radnor, PA). The gas was collected and contained in a three-neck round-bottom 500 mL flask fitted with a rubber septum. Once the flask was filled with CO gas, the remaining formic acid/sulfuric acid solution was poured into 200 mL of cold water to stop the CO formation reaction.

Synthesis of Gold-Coated a-CNCs. Electroless deposition was used to apply additional gold onto the gold nanoparticle-decorated a-CNCs so as to generate continuous gold coatings (i.e., gold nanoshell-bearing CNCs). A suspension of gold nanoparticle-decorated a-CNCs (200 μL, ≈0.006 a-CNC wt % loading) was placed in a 10 mL vial along with a controlled volume (0.1−2.75 mL) of the electroless gold plating solution. DI water was then added to adjust the total suspension volume to 3 mL, and the vial was sealed with a rubber septum. A syringe was used to pull a slight vacuum in the vial to help keep the septum in place during subsequent gold ion reduction, and the contents were briefly mixed with a lab vortexer (Vortex-Genie 2T, Bohemia, NY). A hypodermic needle was then used to inject 1 mL of CO gas just above the suspension within the vial. The vial was quickly placed back on the vortexer and the contents were mixed at the highest speed setting for 1 min. During such mixing, the colorless solution developed a deep purple color, which was consistent with the formation of gold nanoshells. The suspension was then centrifuged (500 RCF) for 10 min. After careful removal of the supernatant, the remaining gold-nanoshell CNCs (AuNS−CNCs) were dispersed in DI water.

Differential Viscosity Gradient Centrifugation. Differential viscosity gradient centrifugation was employed to allow for size/mass-based separation of the AuNS−CNCs. Aqueous solutions of 50, 40, 30, 20, and 10 wt % glycerol were sequentially placed (layer by layer) in a 5 mL centrifuge vial by carefully pipetting solutions of lower glycerol content (lower density) on top of solutions of higher glycerol content (higher density). Each glycerol layer (0.9 mL thick) could be distinguished from the neighboring layers because of the refractive index differences of the layers. The dilute AuNS−CNC suspension was centrifuged down at 500 RCF for 15 min and then dispersed in 100 μL of DI water. This concentrated suspension (≈0.13 wt % AuNS−CNCs) of gold-coated CNCs was then placed on the top (10 wt %) glycerol solution layer, and the vial was centrifuged (300 RCF) for 20 min. Two distinct AuNS−CNCs fractions were recovered. Each fraction was washed (to remove glycerol) using five cycles of centrifugation (1000 RCF, 5 min) and dispersion in DI water. The washed AuNS−CNCs were dispersed in 1 mL of DI water using an ultrasonic bath for 5 min prior to optical analysis.

Fourier Transform Infrared Spectroscopy. Fourier transform infrared spectroscopy (FTIR) analysis was conducted with an Equinox 55 FTIR spectrometer (Bruker, Billerica, MA). Cellulose suspensions (0.01 wt %) were frozen at -80 °C and then freeze-dried (FreeZone 18 lyophilizer, Labconco, Kansas City, MO) for 24 h. The dried samples were mixed with KBr powder (Spectroscopic Grade, Graseby Specac, Orpington, UK) at a concentration of 1 wt % (total mass of 150 mg) and ground into a fine powder mixture in an agate mortar. The KBr−CNC powder mixture was uniaxially pressed into 13.5 mm diameter disks at a peak stress of 550 MPa. The spectral analysis for each sample was obtained as an average of 64 scans conducted in the range of 4000 to 400 cm^{-1} with a resolution of 4 cm^{-1}.

Zeta Potential Analyses. Zeta (ζ) potential analyses of CNC-bearing suspensions were conducted at 25 °C (Nano ZS Zetasizer, Malvern Instruments, Malvern, UK). Prior to such analyses, the suspensions were diluted to a CNC concentration of 0.1 wt % via addition of an aqueous NaCl (1 mM) solution. For each suspension, five analyses were used to obtain an average zeta potential value.

Scanning Electron Microscopy. Scanning electron microscope (SEM) analyses were conducted with a field emission gun instrument (Ultra 60 field emission-SEM, Carl Ziess, Oberkochen, Germany). Samples were prepared by depositing ∼2 μL of Au−CNC suspensions onto ozone-cleaned, platinum-coated silicon wafer substrates and allowing the water to evaporate at room temperature.

Transmission Electron Microscopy. Transmission electron microscope (TEM) analyses of the as-received and gold-decorated CNCs were conducted with a field emission gun instrument (Hitachi HT7700 microscope, Hitachi, Tokyo, Japan) using an accelerating voltage of 120 kV. Dilute CNC suspensions (0.001 wt %) were deposited onto carbon-coated TEM grids (CF300-Cu, Electron Microscopy Sciences, Hatfield, PA) and the water was allowed to evaporate at room temperature. The CNCs were stained by exposure for 3 min to an aqueous solution of 2 wt % uranyl acetate, and the excess liquid was then wicked from the surface using a tissue. TEM analyses of individual AuNS−CNCs were conducted using a LaB_6 filament instrument (Tecnai T20, FEI, Hillsboro, Oregon) at an accelerating voltage of 200 kV. Samples were prepared by depositing 1 μL of dilute (≈0.004 wt %) AuNS−CNC suspension onto carbon-coated copper TEM grids followed by water evaporation at room temperature.

Vis−NIR Spectroscopy. Visible−NIR extinction analyses were conducted with a spectrophotometer (UV-3101PC, Shimadzu, Kyoto, Japan) operating in the range of 400−1300 nm. The spectra of aqueous suspensions were collected over a 1 cm path length using quartz cuvettes (108-QS, Hellma Analytics, Muellheim Germany).

Elemental Analyses. Elemental analyses were conducted to determine the sulfur content in the as-received and desulfated CNC samples (LECO CHNS-932 analyzer, Atlantic Microlabs Inc., Norcross, GA) and the nitrogen content of aminated CNCs (Carlo Erba 1108 elemental analyzer, Atlantic Microlabs Inc.). The CNC specimens were freeze-dried and then vacuum-dried at 60 °C for 24 h prior to analyses.

RESULTS AND DISCUSSION

CNC Surface Functionalization. To create continuous gold coatings on CNCs, it was necessary to alter the CNC surface chemistry to promote gold nanoparticle attachment. In prior gold nanoshell synthesis procedures, aminosilanes have been used to endow templates with an affinity for gold.[6,42,44] However, the ability of silanes present on CNC surfaces to form molecular networks gives rise to the possibility of CNC cross-linking, particularly if the CNCs are not well dispersed. An example of such apparent cross-linking can be seen in the work of Gruber et al., in which gold nanoparticles were deposited on amine-bearing, silica-coated CNCs (the silica coating had been functionalized with aminopropyltriethoxysilane).[40] The TEM images and optical data presented in their work were consistent with agglomerated networks of gold nanoparticle-bearing, silica-coated CNCs and not individually dispersed particles. In the present work, an alternative surface functionalization method was developed to introduce surface amine groups to CNCs, while avoiding such CNC cross-

DOI: 10.1021/acs.langmuir.7b03868
Langmuir 2018, 34, 4427−4436

Scheme 1. Schematic Illustration of the CNC Surface Functionalization Protocol Developed in This Work: (Step 1) Sulfate Half-Ester Removal; (Step 2) Periodate Oxidation; and (Step 3) Reductive Amination (Step 4) Cleavage of the Boc Protecting Group

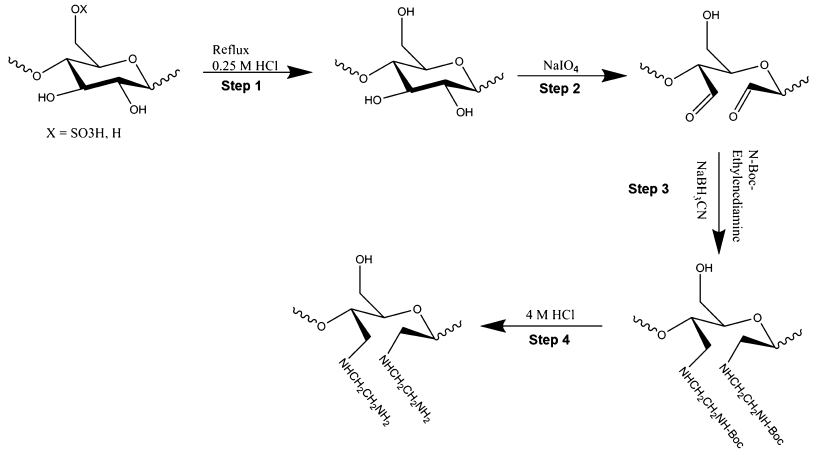

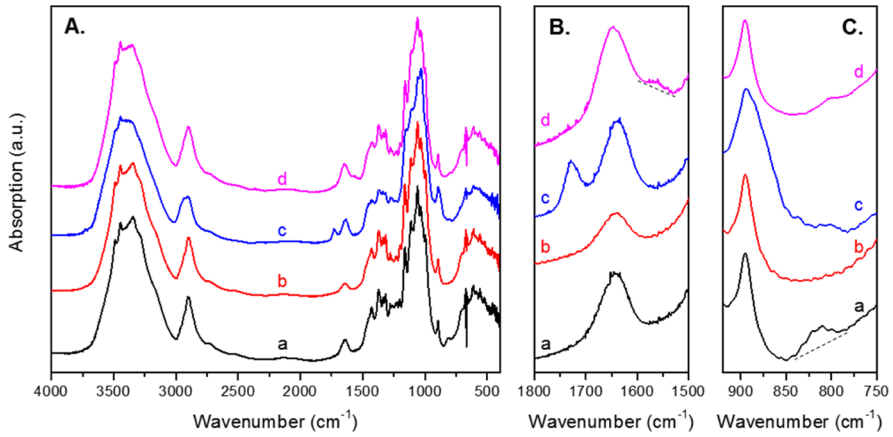

Figure 1. FTIR spectra of CNCs after each functionalization step: (a) as-received CNCs, (b) desulfonated CNCs, (c) dialdehyde-bearing CNCs, and (d) aminated CNCs (a-CNCs). Full wavenumber range (A) and two selected ranges (B,C).

linking. A schematic illustration of this functionalization approach is provided in Scheme 1.

The CNCs used in this work were produced via sulfuric acid hydrolysis of dissolving pulp. During such hydrolysis, some of the native cellulose hydroxyl groups react to form sulfate half-esters.[45] The sulfate ester groups impart a negative surface charge to the CNCs (the average ζ potential of these CNCs was measured in this work to be -40 ± 11 mV at pH 7), which helps to stabilize the particles in suspension. Unfortunately, the amine groups that would be used to bind gold to the CNC surface become protonated, and acquire a net positive charge, under neutral and acidic conditions. The presence of both positively charged amine groups and negatively charged sulfate ester groups on the CNC surfaces would degrade electrostatic repulsion and destabilize the CNC suspensions. To overcome such charge neutralization, a mild hydrochloric acid hydrolysis treatment (Step 1) was conducted to remove the sulfate ester groups prior to surface amination. The efficacy of this HCl treatment was confirmed by ζ potential, elemental sulfur, and FTIR analyses. The ζ potential analyses indicated that this treatment resulted in CNCs with a surface charge of appreciably lower magnitude (-7 ± 4 mV at pH 7) than that for the as-received CNCs (-40 ± 11 mV at pH 7), which was consistent with the removal of sulfate ester groups. Elemental sulfur analyses of the CNCs conducted before and after this HCl treatment yielded values of 0.95 wt % ($\pm$0.3%) and 0.0 wt % ($\pm$0.3%), respectively. FTIR analyses conducted after various stages of the CNC functionalization process are shown in Figure 1. For as-received CNCs, FTIR absorbance located around 1250 cm^{-1} has been attributed to the asymmetrical S=O vibration, whereas a peak around 815 cm^{-1} has been associated with the symmetrical C−O−S vibration.[46] After the HCl treatment, the band that had been located around 815 cm^{-1} in as-received CNCs disappeared (Figure 1), and a decrease ($\approx$35%) in absorbance around 1250 cm^{-1} was also observed, which were consistent with the removal of sulfate ester groups.

A sodium periodate ($NaIO_4$) treatment (Step 2) was then used to oxidize the CNCs to generate dialdehyde groups that, in turn, could undergo subsequent reduction to yield surface amines.[47] A periodate oxidation treatment was chosen over another common CNC oxidation methodology, 2,2,6,6-Tetramethyl-1-piperidinyloxy (TEMPO)-mediated reaction using NaClO, as the latter approach selectively targets only surface C6 hydroxyls, whereas the former (periodate) approach involves the reaction of C2−C3 glycosidic linkages in the cellulose chain. As a result, the periodate reaction can generate more uniformly oxidized crystalline cellulose than the TEMPO-mediated reaction.[47] Indeed, such periodate oxidation of CNCs has been reported to yield a relatively high aldehyde content

DOI: 10.1021/acs.langmuir.7b03868
Langmuir 2018, 34, 4427−4436

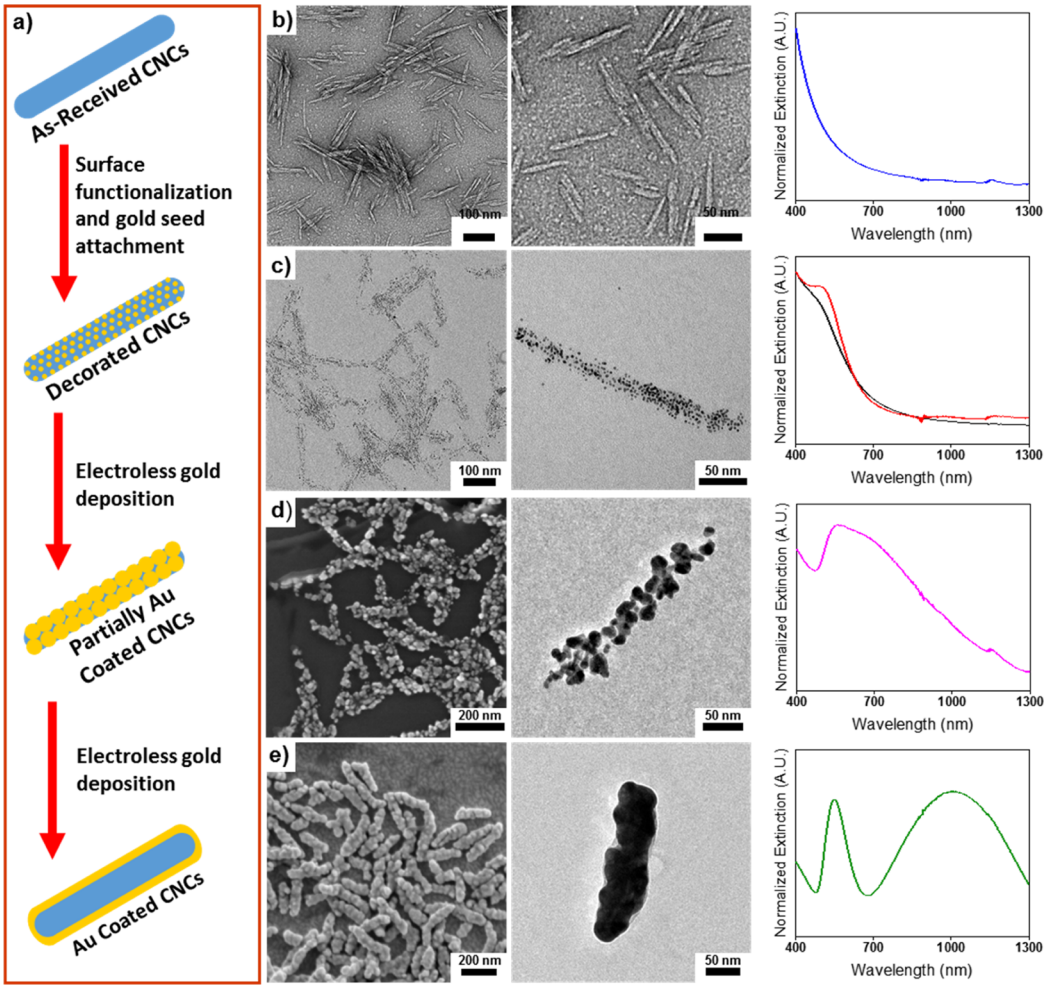

Figure 2. (a) Schematic illustration of the gold coating process. (b) As-received CNCs: TEM images and optical extinction spectrum. (c) Gold-decorated a-CNCs: TEM images and optical extinction spectra of 1−3 nm gold nanoparticles [black] and gold-decorated a-CNCs [red]. (d) Partially gold-coated CNCs: SEM and TEM images of CNCs with partial gold coatings (using 0.25 mL of gold plating solution) and the extinction spectrum. (e) Gold nanoshell-bearing CNCs (AuNS−CNCs): SEM and TEM images of CNCs with complete and continuous gold coatings (using 2.75 mL of gold plating solution) and the extinction spectrum.

(>8 mmol g^{-1}) dictated by the total availability of surface anhydrous glucose units.[47,48] Confirmation of periodate oxidation and surface aldehyde formation on the CNCs of the present work was obtained from FTIR analyses. Comparison of the FTIR spectra obtained before and after periodate-based oxidation of the CNCs (Figure 1) indicated that this treatment resulted in the formation of a peak located at about 1730 cm^{-1} and broadening of the peak located at around 895 cm^{-1}. The new peak at about 1730 cm^{-1} corresponded to a characteristic absorption of the aldehyde carbonyl group, whereas broadening of the 895 cm^{-1} peak was consistent with the formation of hemiacetal bonds between aldehyde groups.[47−49] As expected, ζ-potential measurements of the aldehyde-bearing CNCs yielded an average value (−4 ± 5 mV at pH 7) similar to that for the desulfonated CNCs.

The aldehyde-bearing particles were then exposed to a reductive amination treatment (Step 3). Prior work by Dash et al. and Jin et al. on the reductive amination of aldehydes on CNCs involved the use of a large excess of amine-bearing molecules to push the imine formation reaction far to the right before quickly reducing the imine-bearing products with sodium borohydride.[47,50] In the present case, a molecule possessing multiple amine groups was required for reductive amination, to allow for binding to a given CNC via reaction with a surface aldehyde, while also providing one or more pendant amines for interaction with gold nanoparticles. One concern with the use of such a molecule was the possibility that the amines on a given molecule would react with aldehyde groups present on neighboring CNCs so as to yield cross-linked CNC aggregates. Such cross-linked CNC agglomerates could be quite difficult to disperse in solution, given the low surface charge measured for the dialdehyde-bearing CNCs. Since this work has been aimed at creating single, dispersable CNCs with continuous gold coatings, the reductive amination treatment was conducted with a *tert*-butyloxycarbonyl(Boc)-protected ethylenediamine, so that only one end of this diamine was available for reaction with a surface aldehyde (i.e., only one aldehyde-bearing CNC particle could react with a given (Boc)-protected ethylenediamine molecule). Sodium cyanoborohydride was used as a highly-selective, in situ reductant to convert newly formed imine groups into amines, so as to strongly promote the completion of the reductive amination (aldehyde-consuming) reaction for maximum loading of CNC surfaces with the Boc-protected ethylenediamine.[51] A solution of 4 M HCl was then used to remove the Boc-protecting group, so as to generate CNC particles containing pendant protonated

DOI: 10.1021/acs.langmuir.7b03868
Langmuir 2018, 34, 4427−4436

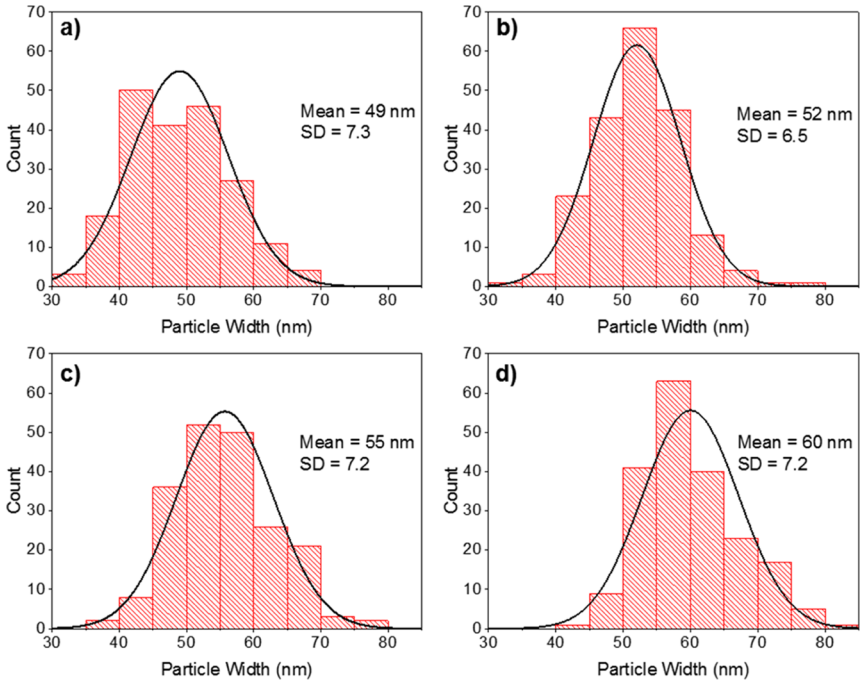

Figure 3. Particle widths of AuNS−CNCs synthesized by exposure to increasing volumes of electroless gold solution: (a) 2.0, (b) 2.125, (c) 2.5, and (d) 2.75 mL.

amine groups for electrostatic CNC repulsion (and good CNC dispersion) and for interaction with gold nanoparticles. The success of this reductive amination process was confirmed by FTIR, ζ-potential, and elemental analyses. Comparison of the FTIR analyses (Figure 1) before and after the reductive amination process indicated that the absorption peak located at around 1730 cm^{-1} disappeared, and the breadth of the peak at around 895 cm^{-1} decreased, after this process which, in turn, were consistent with the removal of the aldehyde carbonyls and the hemiacetal bonds between aldehydes, respectively. The small but detectable increase in infrared absorbance at around 1560 cm^{-1} (Figure 1) was also consistent with absorption because of the N−H bending mode of bound amines.[50] The average ζ-potential value of the aminated CNCs (a-CNCs) was measured to be +33 ± 4 mV at pH 7. This highly-positive a-CNC surface charge was of nearly the same magnitude as the average negative surface charge of the as-received, easily dispersed sulfonated CNCs (−40 ± 11 mV at pH 7). Elemental analyses of the as-received CNCs and the a-CNCs yielded nitrogen contents of 0.0 wt % (±0.3%) and 1.7 wt % (±0.3%), respectively.

Chang et al. have reported that individually dispersed, wood-based CNCs derived from a similar source possessed hydrodynamic radii in the range of 22−27 nm.[52] To evaluate the dispersion and hydrodynamic radii of the a-CNCs formed in the present work, a 0.11 wt % a-CNC suspension was exposed to an ultrasonic probe for various times to break up agglomerates. The state of dispersion/agglomeration of the suspension was assessed by evaluating the average hydrodynamic radius of the a-CNC particles from DLS measurements after various ultrasonication times. After 2 h of ultrasonication, the average hydrodynamic radius of the a-CNCs reached a constant value of 36 nm, which was of similar magnitude as that reported by Chang et al. for individually dispersed CNCs. These individually dispersed a-CNCs served as the starting material for creating gold-coated CNCs.

Synthesis and Optical Properties of Gold-Coated CNCs. Although several methods[53−55] for creating conformal gold coatings on silica shells have been developed, methods similar to those reported by Oldenburg et al.[42,56] were used to apply gold coatings to the a-CNCs of the present work. Briefly, suspensions of a-CNCs and 1−3 nm diameter gold particles were mixed, to allow for the attachment of the gold nanoparticles to the a-CNCs through weak covalent bonding.[57] The CNC-bound gold nanoparticles then served as heterogeneous nucleation sites for subsequent electroless gold deposition. With sufficient electroless deposition, the gold nanoparticles became interconnected to yield continuous nanocrystalline gold shells around the a-CNCs. A schematic illustration of this process is shown in Figure 2a.

TEM analysis of the as-received CNCs (Figure 2b) revealed rod-like particles with a wide distribution of lengths. The optical extinction of the as-received CNC suspensions (Figure 2b) followed a monotonically decaying curve with an increasing wavelength, which is a characteristic of particles exhibiting Rayleigh scattering.[58] Hydrosols of 1−3 nm diameter gold particles whose extinction is dominated by absorption also exhibit a monotonically decaying extinction profile with an increasing wavelength (Figure 2c).[43] The small shoulder seen at 520 nm in the gold hydrosol extinction spectrum was consistent with plasmon absorption associated with particle growth during aging.[43] This plasmon shoulder (Figure 2c) was much more pronounced in the extinction spectrum of gold-decorated a-CNCs, which could be attributed to plasmon coupling between closely spaced gold nanoparticles. TEM images of a-CNCs after gold nanoparticle attachment (Figure 2c) confirmed the presence of rod-like assemblies containing fine gold particles.

To enhance the interconnection of the fine gold nanoparticles along the length of the a-CNCs and to generate a complete gold nanoshell, additional gold was applied via electroless deposition using carbon monoxide (CO) as a

DOI: 10.1021/acs.langmuir.7b03868
Langmuir 2018, 34, 4427−4436

reducing agent. Prior work by Brinson et al. has revealed that the use of CO during such electroless gold deposition enhanced the continuity and uniformity of the resulting gold nanoshells.[42] Heterogeneous gold nucleation during CO-enhanced electroless deposition resulted in coarsening of the gold nanoparticles on the a-CNC surfaces (Figure 2d). After 1 min of exposure to a modest volume of gold electroless solution (0.25 mL), however, significant gaps were still detected between the gold particles on the a-CNC surfaces. Exposure for the same time to a larger volume (>2.0 mL) of gold electroless solution resulted in enhanced gold interconnectivity (Figure 2e) so as to yield a-CNCs possessing complete gold nanoshells (AuNS−CNCs). These particles possessed a zeta potential of −20 ± 4 mV, which is consistent with prior reports for bare gold nanoparticles (previously attributed to the accumulation of hydroxide ions on the gold surface).[59−61]

The extinction spectrum of the AuNS−CNCs exhibited two distinct bands (Figure 2e), with one band located in the visible range (around 550 nm) and the other broader band located in the near-infrared range. These visible and near-infrared bands were consistent with plasmon resonance through the nanoshell thickness and along the nanoshell length, respectively. The broad nature of the near-infrared band in Figure 2e was consistent with the relatively large variation observed in the CNC particle lengths. The position of the near-infrared plasmon peak was highly red-shifted relative to reported longitudinal plasmon resonance peaks for shorter gold nanorods of similar aspect ratio.[62,63] However, such longer/wider gold particles fall outside of the quasi-static dipole approximation range and are subject to phase retardation and plasmon dampening effects, which cause a significant red-shift of the longitudinal plasmon band.[64,65]

Effect of Gold Shell Thickness and Length on Optical Properties. To investigate the influence of the gold nanoshell thickness on the tunability of the longitudinal plasmon band, the amount of deposited gold was increased by exposing gold nanoparticle-decorated a-CNC suspensions of similar concentration and volume (200 μL, ≈0.006 wt % loading) to increasing volumes (2.0 mL to 2.75 mL) of the electroless gold solution. Particle width analyses were then conducted using SEM images of 200 individual particles for each volume of electroless gold solution used. A general increase was observed in the mean AuNS−CNC particle width upon exposure to an increasing volume of electroless gold solution (Figure 3). Student's *t*-test analysis confirmed that within 95% confidence, the values of the mean particle width obtained upon exposure to an increasing volume of electroless solution were statistically different (i.e., *p* values obtained by comparing pairs of data sets were well below 0.001). The values of the average thickness of the gold nanoshells were determined by subtracting the average CNC cross-sectional width value of 7 ± 2 nm (for wood-derived CNCs synthesized via sulfuric acid hydrolysis[66]) from the mean width values shown in Figure 3 and dividing by two. Exposure to an increasing volume of the electroless gold solution (from 2.0 to 2.75 mL) resulted in a monotonic increase in the average thickness of the gold nanoshells (from 21 to 26.5 nm) and, in turn, a monotonic shift in the peak (maximum absorption) location of the longitudinal plasmon band from about 1300 to about 1000 nm (Figure 4).

The width of the longitudinal band also decreased with an increase in the mean gold nanoshell thickness. A similar plasmon resonance behavior has been reported for gold nanoshells[56] as well as gold nanorice[30] and has been attributed

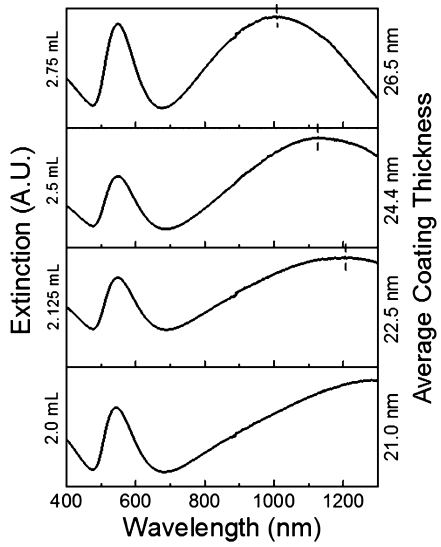

Figure 4. Extinction spectra of gold-coated CNCs showing the effect of the increasing amount of electroless growth solution/average coating thickness (*Y*-axis).

to plasmon mode hybridization[67] between the inner and outer surfaces of the gold nanoshells. Tuning the longitudinal band outside of the range presented here was not investigated because thinner coatings would push the longitudinal plasmon resonance band further into the infrared (which would require a more transparent liquid than water), whereas thicker coatings would reduce the aspect ratio further and produce particles with both extinction bands in the visible wavelength region.

To evaluate the influence of the average gold nanoshell length on the optical behavior, viscosity gradient fractionation was used to obtain populations of AuNS−CNCs with different average nanoshell lengths. A dispersion of AuNS−CNCs prepared with the use of 2.5 mL of electroless gold solution was separated into two fractions, with the population possessing longer AuNS−CNC particles settling at a faster rate. Particle length analyses were conducted using SEM images of 100 individual particles from each fraction. The particle length distributions of the two populations are shown in Figure 5a,c. The average lengths of the two AuNS−CNC populations were 207 nm (±46 nm) and 231 nm (±63 nm), respectively. Although the difference in the average particle length was less than 30 nm, a blue shift of about 100 nm in the longitudinal plasmon band was detected for the AuNS−CNC population with the shorter average particle length. Hence, the plasmonic behavior of the AuNS−CNCs generated in this work could be tailored by controlling the gold coating thickness and/or the CNC length. The gold deposition protocol of the present work may also be applied to other cellulose templates (e.g., CNCs from bacteria or tunicates, or cellulose nanofibrils) with a wider range of aspect ratios.

■ CONCLUSION

This work demonstrates that readily available, biorenewable CNCs can be used as templates for the creation of high aspect ratio gold nanoshell-bearing particles with tunable optical properties. A rational wet chemical approach was developed to generate aminated, positively charged, dispersable, individual CNCs while avoiding appreciable CNC agglomeration. Gold nanoparticles (1−3 nm diameter) were deposited onto the aminated CNCs, and then used as heterogeneous nucleation

DOI: 10.1021/acs.langmuir.7b03868
Langmuir 2018, 34, 4427−4436

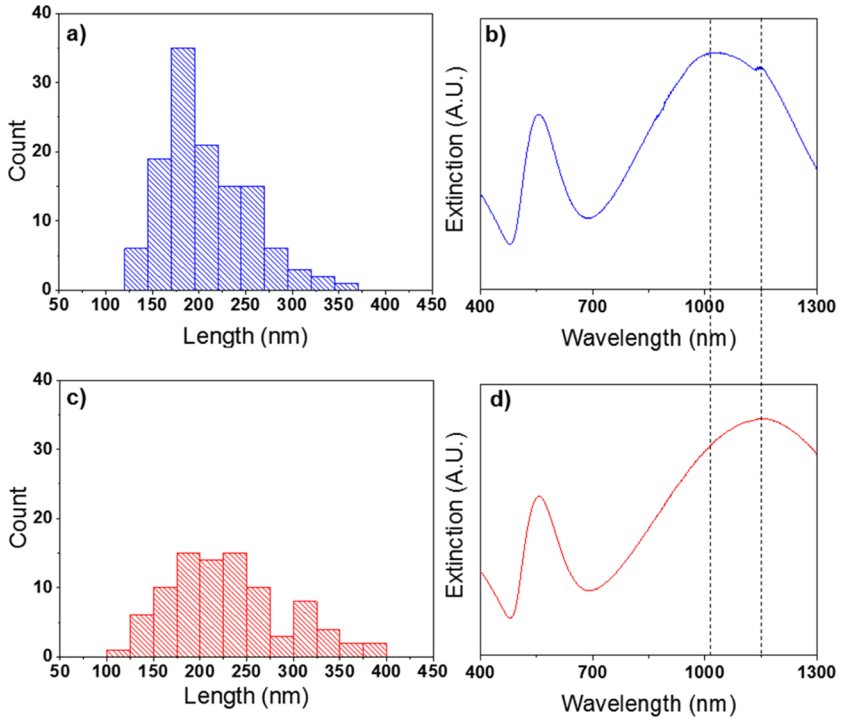

Figure 5. (a,c) Histograms of particle length distributions of the relatively short and long AuNS−CNC fractions. (b,d) Extinction spectra of the relatively short (blue) and long (red) AuNS−CNC fractions.

sites for additional electroless gold deposition to create complete, continuous gold nanoshell coatings on the CNCs. The resulting gold nanoshell-bearing CNCs exhibited two surface plasmon bands that are characteristic of plasmonic core−shell nanostructures. The wavelength location of the NIR (longitudinal) plasmon band could be tuned over a wide range by adjusting the gold coating thickness. The location and width of this NIR band were also found to depend on (and could be tuned by changing) the average length of the CNC templates. The bottom up aqueous synthesis method presented here is a scalable, sustainable, and cost-effective method for creating functional inorganic/bio-organic core−shell structures for a range of potential optical, electrical, catalytic, chemical sensing, and medical applications.

AUTHOR INFORMATION

Corresponding Author

*E-mail: sandhage@purdue.edu.

ORCID

Joseph W. Perry: 0000-0003-1101-7337

Kenneth H. Sandhage: 0000-0002-7957-1361

Notes

The authors declare no competing financial interest.

ACKNOWLEDGMENTS

This research was supported by the Renewable Bioproducts Institute at the Georgia Institute of Technology (CNC functionalization, gold coating, and optical characterization); the U.S. Department of Agriculture (USDA), Forest Products Laboratory (FPL), under award 15-JV-11111129-063 (materials and supplies); the U.S. Department of Energy (DOE), Office of Science, Basic Energy Sciences (BES), under award DE-SC0014034 (optical characterization); and the U.S. Department of Energy (DOE), Office of Energy Efficiency and Renewable Energy, under award DE-EE0007117 (TEM).

REFERENCES

(1) Daniel, M.-C.; Astruc, D. Gold Nanoparticles: Assembly, Supramolecular Chemistry, Quantum-Size-Related Properties, and Applications toward Biology, Catalysis, and Nanotechnology. *Chem. Rev.* **2004**, *104*, 293−346.

(2) Sun, C.; Lee, J.; Zhang, M. Magnetic nanoparticles in MR imaging and drug delivery. *Adv. Drug Delivery Rev.* **2008**, *60*, 1252−1265.

(3) Tong, H.; Ouyang, S.; Bi, Y.; Umezawa, N.; Oshikiri, M.; Ye, J. Nano-photocatalytic Materials: Possibilities and Challenges. *Adv. Mater.* **2012**, *24*, 229−251.

(4) Paul, D. R.; Robeson, L. M. Polymer nanotechnology: Nanocomposites. *Polymer* **2008**, *49*, 3187−3204.

(5) Wang, Y.; Angelatos, A. S.; Caruso, F. Template synthesis of nanostructured materials via layer-by-layer assembly. *Chem. Mater.* **2008**, *20*, 848−858.

(6) Fang, Y.; Chen, V. W.; Cai, Y.; Berrigan, J. D.; Marder, S. R.; Perry, J. W.; Sandhage, K. H. Biologically Enabled Syntheses of Freestanding Metallic Structures Possessing Subwavelength Pore Arrays for Extraordinary (Surface Plasmon-Mediated) Infrared Transmission. *Adv. Funct. Mater.* **2012**, *22*, 2550−2559.

(7) Fang, Y.; Berrigan, J. D.; Cai, Y.; Marder, S. R.; Sandhage, K. H. Syntheses of nanostructured Cu- and Ni-based micro-assemblies with selectable 3-D hierarchical biogenic morphologies. *J. Mater. Chem.* **2012**, *22*, 1305−1312.

(8) Wang, G.; Fang, Y.; Kim, P.; Hayek, A.; Weatherspoon, M. R.; Perry, J. W.; Sandhage, K. H.; Marder, S. R.; Jones, S. C. Layer-By-Layer Dendritic Growth of Hyperbranched Thin Films for Surface Sol−Gel Syntheses of Conformal, Functional, Nanocrystalline Oxide Coatings on Complex 3D (Bio)silica Templates. *Adv. Funct. Mater.* **2009**, *19*, 2768−2776.

(9) Lee, S.-J.; Huang, C.-H.; Shian, S.; Sandhage, K. H. Rapid Hydrolysis of Organophosphorous Esters Induced by Nanostructured, Fluorine-Doped Titania Replicas of Diatom Frustules. *J. Am. Ceram. Soc.* **2007**, *90*, 1632−1636.

DOI: 10.1021/acs.langmuir.7b03868
Langmuir 2018, 34, 4427−4436

(10) Bao, Z.; Weatherspoon, M. R.; Shian, S.; Cai, Y.; Graham, P. D.; Allan, S. M.; Ahmad, G.; Dickerson, M. B.; Church, B. C.; Kang, Z.; Abernathy, H. W., III; Summers, C. J.; Liu, M.; Sandhage, K. H. Chemical reduction of three-dimensional silica micro-assemblies into microporous silicon replicas. *Nature* **2007**, *446*, 172−175.
(11) Zhao, J.; Gaddis, C. S.; Cai, Y.; Sandhage, K. H. Free-standing microscale structures of nanocrystalline zirconia with biologically replicable three-dimensional shapes. *J. Mater. Res.* **2011**, *20*, 282−287.
(12) Gaddis, C. S.; Sandhage, K. H. Freestanding microscale 3D polymeric structures with biologically-derived shapes and nanoscale features. *J. Mater. Res.* **2011**, *19*, 2541−2545.
(13) Zhou, H.; Fan, T.; Zhang, D.; Guo, Q.; Ogawa, H. Novel bacteria-templated sonochemical route for the in situ one-step synthesis of ZnS hollow nanostructures. *Chem. Mater.* **2007**, *19*, 2144−2146.
(14) Tan, S. J.; Campolongo, M. J.; Luo, D.; Cheng, W. Building plasmonic nanostructures with DNA. *Nat. Nanotechnol.* **2011**, *6*, 268−276.
(15) Radloff, C.; Vaia, R. A.; Brunton, J.; Bouwer, G. T.; Ward, V. K. Metal Nanoshell Assembly on a Virus Bioscaffold. *Nano Lett.* **2005**, *5*, 1187−1191.
(16) Dujardin, E.; Peet, C.; Stubbs, G.; Culver, J. N.; Mann, S. Organization of Metallic Nanoparticles Using Tobacco Mosaic Virus Templates. *Nano Lett.* **2003**, *3*, 413−417.
(17) Chen, Y.; Chen, S.; Wang, B.; Yao, J.; Wang, H. TEMPO-oxidized bacterial cellulose nanofibers-supported gold nanoparticles with superior catalytic properties. *Carbohydr. Polym.* **2017**, *160*, 34−42.
(18) Zhang, T.; Wang, W.; Zhang, D.; Zhang, X.; Ma, Y.; Zhou, Y.; Qi, L. Biotemplated Synthesis of Gold Nanoparticle−Bacteria Cellulose Nanofiber Nanocomposites and Their Application in Biosensing. *Adv. Funct. Mater.* **2010**, *20*, 1152−1160.
(19) Meulendijks, N.; Burghoorn, M.; van Ee, R.; Mourad, M.; Mann, D.; Keul, H.; Bex, G.; van Veldhoven, E.; Verheijen, M.; Buskens, P. Electrically conductive coatings consisting of Ag-decorated cellulose nanocrystals. *Cellulose* **2017**, *24*, 2191−2204.
(20) Gomez, I. J.; Goodwin, W. B.; Sabo, D.; Zhang, Z. J.; Sandhage, K. H.; Meredith, J. C. Three-dimensional magnetite replicas of pollen particles with tailorable and predictable multimodal adhesion. *J. Mater. Chem. C* **2015**, *3*, 632−643.
(21) Goodwin, W. B.; Gomez, I. J.; Fang, Y.; Meredith, J. C.; Sandhage, K. H. Conversion of Pollen Particles into Three-Dimensional Ceramic Replicas Tailored for Multimodal Adhesion. *Chem. Mater.* **2013**, *25*, 4529−4536.
(22) Savage, K. J.; Hawkeye, M. M.; Esteban, R.; Borisov, A. G.; Aizpurua, J.; Baumberg, J. J. Revealing the quantum regime in tunnelling plasmonics. *Nature* **2012**, *491*, 574−577.
(23) Kochuveedu, S. T.; Jang, Y. H.; Kim, D. H. A study on the mechanism for the interaction of light with noble metal-metal oxide semiconductor nanostructures for various photophysical applications. *Chem. Soc. Rev.* **2013**, *42*, 8467−8493.
(24) Dreaden, E. C.; Alkilany, A. M.; Huang, X.; Murphy, C. J.; El-Sayed, M. A. The golden age: gold nanoparticles for biomedicine. *Chem. Soc. Rev.* **2012**, *41*, 2740−2779.
(25) Saha, K.; Agasti, S. S.; Kim, C.; Li, X.; Rotello, V. M. Gold Nanoparticles in Chemical and Biological Sensing. *Chem. Rev.* **2012**, *112*, 2739−2779.
(26) Corma, A.; Garcia, H. Supported gold nanoparticles as catalysts for organic reactions. *Chem. Soc. Rev.* **2008**, *37*, 2096−2126.
(27) Smith, A. M.; Mancini, M. C.; Nie, S. Bioimaging: Second window for in vivo imaging. *Nat. Nanotechnol.* **2009**, *4*, 710−711.
(28) Tong, L.; Wei, Q.; Wei, A.; Cheng, J.-X. Gold Nanorods as Contrast Agents for Biological Imaging: Optical Properties, Surface Conjugation and Photothermal Effects. *Photochem. Photobiol.* **2009**, *85*, 21−32.
(29) Ye, S.; Marston, G.; McLaughlan, J. R.; Sigle, D. O.; Ingram, N.; Freear, S.; Baumberg, J. J.; Bushby, R. J.; Markham, A. F.; Critchley, K.; Coletta, P. L.; Evans, S. D. Engineering Gold Nanotubes with Controlled Length and Near-Infrared Absorption for Theranostic Applications. *Adv. Funct. Mater.* **2015**, *25*, 2117−2127.
(30) Wang, H.; Brandl, D. W.; Le, F.; Nordlander, P.; Halas, N. J. Nanorice: A Hybrid Plasmonic Nanostructure. *Nano Lett.* **2006**, *6*, 827−832.
(31) Jain, P. K.; Huang, X.; El-Sayed, I. H.; El-Sayed, M. A. Noble Metals on the Nanoscale: Optical and Photothermal Properties and Some Applications in Imaging, Sensing, Biology, and Medicine. *Acc. Chem. Res.* **2008**, *41*, 1578−1586.
(32) Gobin, A. M.; Lee, M. H.; Halas, N. J.; James, W. D.; Drezek, R. A.; West, J. L. Near-infrared resonant nanoshells for combined optical imaging and photothermal cancer therapy. *Nano Lett.* **2007**, *7*, 1929−1934.
(33) Lusic, H.; Grinstaff, M. W. X-ray-Computed Tomography Contrast Agents. *Chem. Rev.* **2013**, *113*, 1641−1666.
(34) Astolfo, A.; Arfelli, F.; Schültke, E.; James, S.; Mancini, L.; Menk, R.-H. A detailed study of gold-nanoparticle loaded cells using X-ray based techniques for cell-tracking applications with single-cell sensitivity. *Nanoscale* **2013**, *5*, 3337−3345.
(35) Hainfeld, J. F.; Slatkin, D. N.; Focella, T. M.; Smilowitz, H. M. Gold nanoparticles: a new X-ray contrast agent. *Br. J. Radiol.* **2006**, *79*, 248−253.
(36) Postek, M. T.; Moon, R. J.; Rudie, A. W.; Bilodeau, M. A. *Production and Applications of Cellulose*; Tappi Press: Peachtree Corners, 2013.
(37) Moon, R. J.; Martini, A.; Nairn, J.; Simonsen, J.; Youngblood, J. Cellulose nanomaterials review: structure, properties and nanocomposites. *Chem. Soc. Rev.* **2011**, *40*, 3941−3994.
(38) Habibi, Y. Key advances in the chemical modification of nanocelluloses. *Chem. Soc. Rev.* **2014**, *43*, 1519−1542.
(39) Padalkar, S.; Capadona, J. R.; Rowan, S. J.; Weder, C.; Won, Y.-H.; Stanciu, L. A.; Moon, R. J. Natural Biopolymers: Novel Templates for the Synthesis of Nanostructures. *Langmuir* **2010**, *26*, 8497−8502.
(40) Gruber, S.; Taylor, R. N. K.; Scheel, H.; Greil, P.; Zollfrank, C. Cellulose-biotemplated silica nanowires coated with a dense gold nanoparticle layer. *Mater. Chem. Phys.* **2011**, *129*, 19−22.
(41) Alkilany, A. M.; Nagaria, P. K.; Hexel, C. R.; Shaw, T. J.; Murphy, C. J.; Wyatt, M. D. Cellular Uptake and Cytotoxicity of Gold Nanorods: Molecular Origin of Cytotoxicity and Surface Effects. *Small* **2009**, *5*, 701−708.
(42) Brinson, B. E.; Lassiter, J. B.; Levin, C. S.; Bardhan, R.; Mirin, N.; Halas, N. J. Nanoshells Made Easy: Improving Au Layer Growth on Nanoparticle Surfaces. *Langmuir* **2008**, *24*, 14166−14171.
(43) Duff, D. G.; Baiker, A.; Edwards, P. P. A new hydrosol of gold clusters. 1. Formation and particle size variation. *Langmuir* **1993**, *9*, 2301−2309.
(44) Pham, T.; Jackson, J. B.; Halas, N. J.; Lee, T. R. Preparation and Characterization of Gold Nanoshells Coated with Self-Assembled Monolayers. *Langmuir* **2002**, *18*, 4915−4920.
(45) Eyley, S.; Thielemans, W. Surface modification of cellulose nanocrystals. *Nanoscale* **2014**, *6*, 7764−7779.
(46) Gu, J.; Catchmark, J. M.; Kaiser, E. Q.; Archibald, D. D. Quantification of cellulose nanowhiskers sulfate esterification levels. *Carbohydr. Polym.* **2013**, *92*, 1809−1816.
(47) Jin, L.; Li, W.; Xu, Q.; Sun, Q. Amino-functionalized nanocrystalline cellulose as an adsorbent for anionic dyes. *Cellulose* **2015**, *22*, 2443−2456.
(48) Azzam, F.; Galliot, M.; Putaux, J.-L.; Heux, L.; Jean, B. Surface peeling of cellulose nanocrystals resulting from periodate oxidation and reductive amination with water-soluble polymers. *Cellulose* **2015**, *22*, 3701−3714.
(49) Kim, U.-J.; Kuga, S.; Wada, M.; Okano, T.; Kondo, T. Periodate Oxidation of Crystalline Cellulose. *Biomacromolecules* **2000**, *1*, 488−492.
(50) Dash, R.; Elder, T.; Ragauskas, A. J. Grafting of model primary amine compounds to cellulose nanowhiskers through periodate oxidation. *Cellulose* **2012**, *19*, 2069−2079.

DOI: 10.1021/acs.langmuir.7b03868
Langmuir 2018, 34, 4427−4436

(51) Lane, C. F. Sodium Cyanoborohydride - A Highly Selective Reducing Agent for Organic Functional Groups. *Synthesis* **1975**, *1975*, 135−146.
(52) Chang, H.; Luo, J.; Davijani, A. A. B.; Chien, A.-T.; Wang, P.-H.; Liu, H. C.; Kumar, S. Individually Dispersed Wood-Based Cellulose Nanocrystals. *ACS Appl. Mater. Interfaces* **2016**, *8*, 5768−5771.
(53) Priyam, A.; Idris, N. M.; Zhang, Y. Gold nanoshell coated $NaYF_4$ nanoparticles for simultaneously enhanced upconversion fluorescence and darkfield imaging. *J. Mater. Chem.* **2012**, *22*, 960−965.
(54) Brito-Silva, A. M.; Sobral-Filho, R. G.; Barbosa-Silva, R.; de Araujo, C. B.; Galembeck, A.; Brolo, A. G. Improved Synthesis of Gold and Silver Nanoshells. *Langmuir* **2013**, *29*, 4366−4372.
(55) Watanabe, S.; Hiratsuka, T.; Asahi, Y.; Tanaka, A.; Mae, K.; Miyahara, M. T. Flow Synthesis of Plasmonic Gold Nanoshells via a Microreactor. *Part. Part. Syst. Charact.* **2015**, *32*, 234−242.
(56) Oldenburg, S. J.; Averitt, R. D.; Westcott, S. L.; Halas, N. J. Nanoengineering of optical resonances. *Chem. Phys. Lett.* **1998**, *288*, 243−247.
(57) Leff, D. V.; Brandt, L.; Heath, J. R. Synthesis and characterization of hydrophobic, organically-soluble gold nanocrystals functionalized with primary amines. *Langmuir* **1996**, *12*, 4723−4730.
(58) Bohren, C. F.; Huffman, D. R. Absorption and Scattering by an Arbitrary Particle. *Absorption and Scattering of Light by Small Particles*; Wiley-VCH Verlag GmbH, 2007; pp 57−81.
(59) Csapo, E.; Sebok, D.; Babic, J. M.; Supljika, F.; Bohus, G.; Dekany, I.; Kallay, N.; Preocanin, T. Surface and Structural Properties of Gold Nanoparticles and Their Biofunctionalized Derivatives in Aqueous Electrolytes Solution. *J. Dispersion Sci. Technol.* **2014**, *35*, 815−825.
(60) Verwey, E. J. W.; de Boer, J. H. Surface oxide films. *Recl. Trav. Chim. Pays-Bas* **1936**, *55*, 675−687.
(61) Pfeiffer, C.; Rehbock, C.; Huhn, D.; Carrillo-Carrion, C.; de Aberasturi, D. J.; Merk, V.; Barcikowski, S.; Parak, W. J. Interaction of colloidal nanoparticles with their local environment: the (ionic) nanoenvironment around nanoparticles is different from bulk and determines the physico-chemical properties of the nanoparticles. *J. R. Soc., Interface* **2014**, *11*, 20130931.
(62) Eustis, S.; El-Sayed, M. A. Determination of the aspect ratio statistical distribution of gold nanorods in solution from a theoretical fit of the observed inhomogeneously broadened longitudinal plasmon resonance absorption spectrum. *J. Appl. Phys.* **2006**, *100*, 044324.
(63) Link, S.; Mohamed, M. B.; El-Sayed, M. A. Simulation of the Optical Absorption Spectra of Gold Nanorods as a Function of Their Aspect Ratio and the Effect of the Medium Dielectric Constant. *J. Phys. Chem. B* **1999**, *103*, 3073−3077.
(64) Encina, E. R.; Coronado, E. A. Resonance Conditions for Multipole Plasmon Excitations in Noble Metal Nanorods. *J. Phys. Chem. C* **2007**, *111*, 16796−16801.
(65) Slaughter, L. S.; Chang, W.-S.; Swanglap, P.; Tcherniak, A.; Khanal, B. P.; Zubarev, E. R.; Link, S. Single-Particle Spectroscopy of Gold Nanorods beyond the Quasi-Static Limit: Varying the Width at Constant Aspect Ratio. *J. Phys. Chem. C* **2010**, *114*, 4934−4938.
(66) Reid, M. S.; Villalobos, M.; Cranston, E. D. Benchmarking Cellulose Nanocrystals: From the Laboratory to Industrial Production. *Langmuir* **2017**, *33*, 1583−1598.
(67) Prodan, E.; Radloff, C.; Halas, N. J.; Nordlander, P. A Hybridization Model for the Plasmon Response of Complex Nanostructures. *Science* **2003**, *302*, 419−422.

DOI: 10.1021/acs.langmuir.7b03868
Langmuir 2018, 34, 4427−4436